

## EDGE DEBONDING IN FRP-STRENGTHENED CONCRETE BEAMS: AN ANALYTICAL APPROACH BASED ON THE COHESIVE CRACK MODEL

P. CORNETTI<sup>\*</sup>, M. CORRADO<sup>\*</sup>, L. DE LORENZIS<sup>†</sup> AND A. CARPINTERI<sup>\*</sup>

<sup>\*</sup> Politecnico di Torino

Department of Structural, Geotechnical and Building Engineering

Corso Duca degli Abruzzi 24, 10129 Torino, Italy

e-mail: pietro.cornetti@polito.it, mauro.corrado@polito.it, alberto.carpinteri@polito.it

<sup>†</sup> Università del Salento

Department of Innovation Engineering

Via per Monteroni s/n, 73100, Lecce, Italy

e-mail: laura.delorenzis@unisalento.it

**Key words:** Cohesive Model, Edge Debonding, Fracture Mechanics, FRP, Plate-end Debonding.

**Abstract:** This paper focuses on the prediction of edge debonding for a concrete beam retrofitted with a fiber-reinforced polymer plate. This failure mechanism, also known in the literature as plate-end debonding, stems from the concentration of interfacial stresses arising at the termination of the strengthening plate. Early models of edge debonding adopted failure criteria based on interfacial stresses. However, due to the typically catastrophic nature of this failure mechanism, approaches based on linear elastic fracture mechanics (LEFM) are becoming increasingly established. In this paper, the problem is addressed by means of the cohesive crack model. This model is able to bridge the gap between the stress- and the energy-based approaches and nevertheless has been used in a very limited number of analytical studies to date. Based on a cohesive interface law with linear softening, closed-form solutions for the interfacial stresses and the load-displacement curves, as well as for the ultimate load, are derived. A parametric analysis shows that for sufficiently brittle interfaces both snap-back and snap-through instabilities may arise. As the interface ductility increases, the snap-back disappears and finally a monotonic load-displacement curve is obtained. LEFM is shown to provide unconservative estimates, which justifies the need for the proposed approach.

### 1 INTRODUCTION

Among the strengthening techniques for civil engineering structures and in particular for concrete structures, bonding of fiber-reinforced polymer (FRP) sheets is nowadays widely employed. The advantages of this technique are several. FRP laminates are easy to install and cause a minimal increase in size of the structure; furthermore, they possess high strength, light weight and excellent durability.

The structural behaviour of FRP-strengthened members is substantially different from that of the original

unstrengthened members and, even more importantly, new failure modes may occur [1-2]. Among the observed failure modes, the so-called edge debonding of the FRP plate (also known as plate-end debonding) deserves a special attention because of its catastrophic nature. The present paper focuses on the analytical prediction of this failure mechanism.

Early predictive models of edge debonding failure were based on setting limits for the stresses at the FRP-concrete interface [3-4]. However, because of the brittleness of the debonding process, an energy approach seems

to be more effective, since stress-based failure criteria are more suitable for gradual and ductile failures. Energy-based fracture criteria have been recently proposed by Rabinovitch [5], Colombi [6] and Carpinteri et al. [7] by applying the Linear Elastic Fracture Mechanics (LEFM) concept of strain energy release rate.

With the objective to bridge the gap between the stress- and energy-based approaches, in the present paper the problem is addressed by means of the cohesive crack model. While several investigations on the debonding process in FRP-concrete joints subjected to pure shear have adopted the cohesive crack model either in analytical [8-12] or in numerical form [13-14], limited studies have been conducted on cohesive crack modeling of interfacial stresses in plated beams [15-18]. While Refs. [15] and [18] focus on numerical methods, Refs. [16] and [17] present the first cohesive crack analytical solutions for edge debonding of a beam under three-point bending (TPB) and constant bending moment, respectively.

The present work focuses on edge debonding of an FRP strengthened beam under a TPB loading condition, extending previous results given in Carpinteri et al. [7] and De Lorenzis & Zavarise [16]. After derivation of the interfacial stresses during the various stages of the interfacial behavior, the attention is focused on the load vs. mid-span deflection curves, thereby highlighting the possible occurrence of snap-back and snap-through instabilities. A closed-form implicit formula for the value of the load causing unstable propagation of the debonding crack according to the cohesive model is derived and discussed.

Throughout this paper, linear-elastic behavior for all materials is assumed and all non-linearities are concentrated at the interface. While being an oversimplification of the actual behavior, this assumption is suitable to highlight the essential features of the debonding process and the role played by the most significant variables.

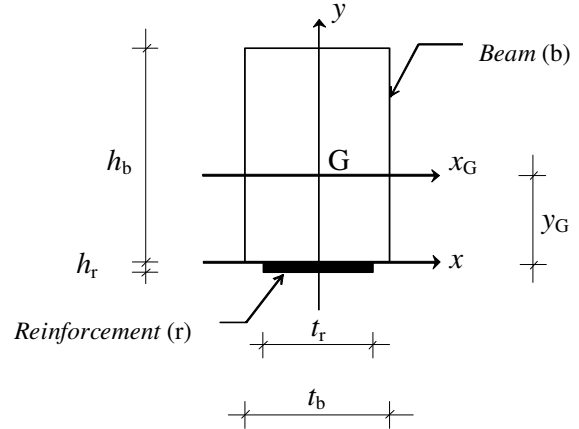


Figure 1: Geometry of the strengthened cross section.

## 2 EQUIVALENT BEAM MODEL AND LINEAR ELASTIC FRACTURE MECHANICS

The easiest model for plated beams is the so-called equivalent beam (EB) model, based on the assumption of a planar cross section for the whole structure. Let us refer to a beam with a rectangular cross section (Fig. 1) strengthened by an FRP strip at its bottom. In the following, the quantities with subscript “b” refer to the beam to be strengthened and the ones with subscript “r” to the reinforcement. Thus  $E_b$ ,  $E_r$  are the Young moduli of the beam and of the reinforcement;  $h_b$ ,  $h_r$  are their respective thicknesses;  $t_b$  and  $t_r$  their widths. The mechanical percentage of reinforcement is therefore:

$$\rho = \frac{E_r h_r t_r}{E_b h_b t_b} \quad (1)$$

Usually, the thickness of the FRP strip is at least two orders of magnitude smaller than the beam height. Hence, when computing the centre of gravity and the moment of inertia of the reinforced section, the powers of the  $h_b/h_r$  ratio with exponent greater than or equal to two can be neglected if compared to unity. Thus the position  $y_G$  of the centre of gravity of the reinforced section (with respect to the bottom of the beam) and its moment of inertia (with respect to the  $x_G$  axis) read (Fig. 1):

$$y_G = \frac{h_b}{2(1+\rho)} \quad (1)$$

$$I = \frac{1+4\rho}{1+\rho} I_b \quad (2)$$

where  $I_b = t_b h_b^3 / 12$  is the moment of inertia of the plain beam section.

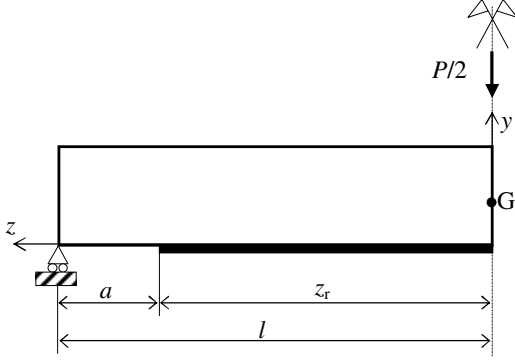


**Figure 2:** An FRP-strengthened beam in a three point bending configuration. Symmetry is exploited to study only half of the structure.

Let us consider a TPB geometry (Fig. 2). The beam span is  $2l$  and  $P$  is the concentrated load. The length of the FRP strip (i.e. the initial bond length) is  $2z_r$ . If  $z$  is the axial coordinate with origin at the beam mid-span, on the left side of the beam the shear force is  $T = P/2$  and the bending moment is  $M = -P(l-z)/2$ .

For fixed load conditions, the strain energy release rate is given by the derivative of the strain energy with respect to the crack area  $A$ , which is equal to the product of the crack length  $a$  times its width  $t_r$ . Hence, the equivalent beam model yields:

$$\mathcal{G} = \frac{d\Phi}{dA} = \frac{1}{t_r} \left[ \frac{M^2}{2E_b I_b} - \frac{M^2}{2E_b I} \right]_{z=z_r} \quad (3)$$

Hence, by eqn (2):

$$\mathcal{G} = \frac{9\rho}{2(1+4\rho)} \frac{P^2(l-z_r)^2}{t_r t_b h_b^3 E_b} \quad (4)$$

According to LEFM, debonding occurs whenever  $\mathcal{G}$  reaches its critical value  $\mathcal{G}_c$ , i.e. the fracture energy. The failure load  $P_{LEFM}$  is

therefore:

$$P_{LEFM} = \frac{\sqrt{1+4\rho}}{3\rho} \frac{t_r h_b}{l-z_r} \sqrt{2\mathcal{G}_c E_b t_r} \quad (5)$$

Eqn (5) shows that the debonding process is unstable, since the load causing the FRP debonding decreases as the bond length  $z_r$  decreases. This catastrophic behavior, typical of plated beams failing by edge debonding, explains the considerable attention of researchers on this failure mechanism. In the following sections, a new estimate for the edge debonding load will be given on the basis of a more refined, although still analytical, model. It will also be shown that the LEFM estimate (5) is an upper bound. Thus, although LEFM is able to provide by a simple formula a rough estimate of the debonding load, it must be emphasized that this value does not represent a conservative prediction.

According to the EB model, the elementary beam theory provides the following value for the mid-span deflection  $v_{EB}$ :

$$v_{EB} = \frac{P(2l)^3}{48E_b I} \left[ 1 + \frac{3\rho}{1+\rho} \left( 1 - \frac{z_r}{l} \right)^3 \right] \quad (6)$$

where the term outside the square bracket represents the mid-span deflection if the beam were reinforced over the whole span; or, equivalently, the second term inside the square bracket represents the relative increment of deformability due to a bond length  $z_r$  shorter than the beam length  $l$ .

For an ideal test where it is possible to control the advancement of the debonding crack (i.e.  $z_r$ ), the load-displacement curve is simply given by eqns (5) and (6) (provided that eqn (5) is substituted into eqn (6)) while the bond length decreases from its initial value to zero. A typical plot is drawn in fig. 3, where the load and the displacement have been normalized by their respective values at the onset of debonding. After a linear elastic loading phase, debonding starts and it ends when the FRP plate is completely detached. Then the load can increase again, the loading curve being now represented by the straight line characterizing the linear elastic behavior

of the unstrengthened beam. Up to a multiplicative factor, the area between the thick curve and the dashed line represents the energy spent to separate the reinforcement from the beam. It is evident that a snap-through instability occurs if the test is load-controlled and that a snap-back instability takes place if the test is mid-span displacement-controlled.

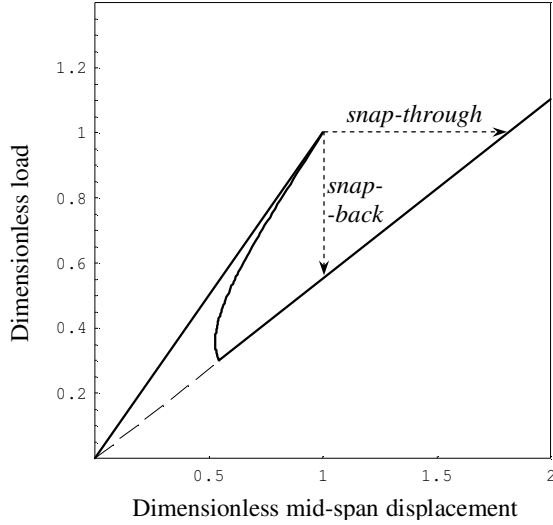


**Figure 3:** Dimensionless load vs. displacement curve according to LEFM ( $\rho = 0.4$ ,  $z_r/l = 0.7$ ).

### 3 GOVERNING EQUATIONS

The EB model presented in the previous section does not take into account the interface compliance nor its softening behavior. It is easily argued that, wishing to tackle the debonding process, a more realistic description of the FRP-concrete interface is needed. Since our goal is the development of an analytical model, we introduce the simplifying assumption that the interface works as a shear lag, i.e. it transfers stresses from the beam to the FRP reinforcement by means of tangential stresses only. In other words we are neglecting the peeling stresses, an assumption that in the present geometry appears reasonable due to the small bending stiffness of the FRP reinforcement.

While in the EB model the section of the composite beam is assumed to be planar, in the present model cross sections remain planar

after deformation only inside the beam:

$$w_b(y, z) = w_{b0}(z) + \varphi_b(z) y \quad (7)$$

where  $w_b$  is the axial displacement field of the beam,  $\varphi_b$  is the rotation of the cross section at the distance  $z$  from the mid-span and  $w_{b0}$  is the axial displacement of the points at the bottom of the beam. Denoting by  $\varepsilon_b$  and  $\varepsilon_r$  the strains of the beam and the reinforcement, respectively, and by  $w_r$  the axial displacement of the reinforcement, the assumption of a linear elastic behaviour for concrete and the reinforcement yields:

$$\begin{aligned} \sigma_b &= E_b \varepsilon_b = E_b \left( \frac{dw_{b0}}{dz} + \frac{d\varphi_b}{dz} y \right) = \\ &= E_b (\varepsilon_{b0} + \chi_b y) \end{aligned} \quad (8)$$

$$\sigma_r = E_r \varepsilon_r = E_r \frac{dw_r}{dz} \quad (9)$$

where  $\chi_b$  is the beam curvature and  $\varepsilon_{b0}$  is the strain at the beam intrados. On the other hand, the shear stress  $\tau(s)$  at the interface is assumed to be a function (which will be specified in the next section) of the relative displacement  $s$  between the FRP and the beam intrados:

$$s = w_{b0} - w_r \quad (10)$$

The normal stress distribution along each cross section has to be equivalent to the axial force (which is equal to zero) and to the bending moment  $M$ . In formulae:

$$\int_0^{h_b} \sigma_b t_b dy + \sigma_r t_r h_r = 0 \quad (11)$$

$$\int_0^{h_b} \sigma_b y t_b dy = M \quad (12)$$

where the contribution of the reinforcement to the bending moment has been neglected due to its small thickness. Substituting eqns (8-9) into eqns (11-12), two algebraic equations are obtained from which it is possible to express the strain at the bottom of the beam and the beam curvature as a function of the strain in the FRP:

$$\varepsilon_{b0} = \frac{3P}{t_b h_b^2 E_b} (l - z) - 4\rho \varepsilon_r \quad (13)$$

$$\chi_b = \frac{6\rho \varepsilon_r}{h_b} - \frac{6P}{t_b h_b^3 E_b} (l - z) \quad (14)$$

It is now convenient to express all the unknown variables as functions of the relative displacement  $s$ . Deriving eqn (10) and using eqn (13) yields:

$$\varepsilon_r = \frac{1}{1+4\rho} \left[ \frac{3P(l-z)}{t_b h_b^2 E_b} - \frac{ds}{dz} \right] \quad (15)$$

The longitudinal equilibrium equation of the FRP strip is:

$$h_r \frac{d\sigma_r}{dz} + \tau(s) = 0 \quad (16)$$

Deriving eqn (15) and substituting the result into eqn (16) together with eqn (9), the final governing second order differential equation in the unique unknown variable  $s$  is obtained:

$$\frac{d^2 s}{dz^2} - \frac{1+4\rho}{E_r h_r} \tau(s) = -\frac{3P}{t_b h_b^2 E_b} \quad (17)$$

#### 4 COHESIVE LAW OF THE INTERFACE

The interface is assumed to be macroscopically described by the  $\tau$  vs.  $s$  function. Such a relation takes into account the shear deformability and the progressive damage mechanisms taking place both in the adhesive layer used to bond the FRP sheet to the concrete, and in the superficial layer of the beam involved by the interfacial stress transfer [13].

Here we assume that the mechanical behavior of the interface can be satisfactorily described by a bi-linear law as represented in Fig.4:  $\tau_p$  is the peak stress,  $s_p$  the corresponding relative displacement and  $s_f$  the final relative displacement, i.e. the value after which the reinforcement is considered completely detached from the concrete beam. The initial (elastic) stiffness of the interface is denoted by  $k = \tau_p/s_p$  and the interfacial fracture energy is equal to  $G_c = \tau_p s_f / 2$ . Introducing the

ratio  $\mu = s_f / s_p$  and the dimensionless relative displacement  $\delta = s/s_p$ , the cohesive law can be given analytically as:

$$\frac{\tau}{\tau_p} = f(\delta) = \begin{cases} \delta, & \text{if } 0 \leq \delta \leq 1 \\ \mu - \delta, & \text{if } 1 < \delta \leq \mu \\ 0, & \text{if } \delta > \mu \end{cases} \quad (18)$$

By normalizing the axial coordinate and the length of the FRP with respect to the beam length, i.e.  $\zeta = z/l$  and  $\zeta_r = z_r/l$ , and the load with respect to the LEFM estimate (5), i.e.  $\Pi = P/P_{LEFM}$ , the governing equation can be set in dimensionless form as:

$$\frac{d^2 \delta}{d\zeta^2} - \alpha^2 f(\delta) = -\frac{\alpha \sqrt{\mu}}{1-\zeta_r} \Pi \quad (19)$$

where the dimensionless parameter  $\alpha$  depends on the geometric and elastic properties of the materials. It is worth observing that, up to the factor  $(1+4\rho)$ ,  $\alpha^2$  can be seen as the ratio between the tangential stiffness of the interface and the axial stiffness of the reinforcement:

$$\alpha^2 = (1+4\rho) \frac{k l^2}{E_r h_r} \quad (20)$$

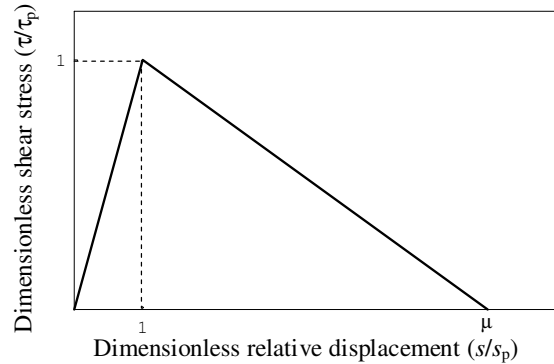


Figure 4: Interfacial cohesive law with linear softening.

#### 5 ANALYSIS OF THE INTERFACE BEHAVIOR

In this section we analyze the evolution of the stress and displacement fields along the interface during loading. This process consists in three stages: the elastic stage, the elastic-softening stage and the elastic-softening-

debonding stage.

### 5.1 Elastic stage

During the first stage the whole length of the interface is in the elastic regime ( $\delta < 1$ ). The boundary conditions prescribe a null relative displacement at the mid-span (because of symmetry) as well as a vanishing axial stress in the reinforcement at its edge, i.e.  $\varepsilon_r = 0$  at  $z = z_r$ . By means of eqn (15), the differential problem (19) becomes:

$$\begin{cases} \frac{d^2\delta}{d\zeta^2} - \alpha^2 \delta = -\frac{\alpha\sqrt{\mu}}{1-\zeta_r} \Pi, & 0 \leq \zeta \leq \zeta_r \\ \delta(0) = 0, \quad \delta'(\zeta_r) = \Pi\alpha\sqrt{\mu} \end{cases} \quad (21)$$

yielding:

$$\delta(\zeta) = \frac{\Pi\sqrt{\mu}}{\alpha(1-\zeta_r)} \cdot \left\{ 1 + \frac{\alpha(1-\zeta_r)\sinh(\alpha\zeta) - \cosh[\alpha(\zeta_r - \zeta)]}{\cosh(\alpha\zeta_r)} \right\} \quad (22)$$

It is evident that the interfacial relative displacement, as well as the shear stress, increase monotonically along the axial coordinate, reaching the maximum value at the FRP edge. Since the interface is still completely elastic, the stress and displacement fields are both proportional to the applied load. The elastic stage ends when the shear stress reaches the peak value of the cohesive law, i.e. when  $\delta(\zeta_r) = 1$ . We denote by  $\Pi_{el}$  the corresponding limit elastic load, which, according to eqn (22), is equal to:

$$\Pi_{el} = \frac{\alpha(1-\zeta_r) \cosh(\alpha\zeta_r)}{\sqrt{\mu} [\cosh(\alpha\zeta_r) + \alpha(1-\zeta_r)\sinh(\alpha\zeta_r) - 1]} \quad (23)$$

### 5.2 Elastic-softening stage

Once the interfacial shear stress reaches the peak value at the termination of the plate, the interface enters the elastic-softening stage and the shear stress peak starts moving from the edge towards the mid-span. We denote the (dimensionless) position of the peak by  $\bar{\zeta}$ . This parameter controls the debonding process. During the elastic-softening stage,  $\bar{\zeta}$

decreases from  $\zeta_r$  to  $\zeta_{23}$ , the latter being the value (computed later) at which the second stage ends and the third one begins.

During this second stage, the central portion of the reinforcement is still in elastic conditions, whereas the regions close to the edges have entered the softening regime but are not yet debonded from the substrate. It is therefore necessary to solve two differential problems. The first one refers to the elastic zone:

$$\begin{cases} \frac{d^2\delta}{d\zeta^2} - \alpha^2 \delta = -\frac{\alpha\sqrt{\mu}}{1-\zeta_r} \Pi, & 0 \leq \zeta < \bar{\zeta} \\ \delta(0) = 0, \quad \delta(\bar{\zeta}) = 1 \end{cases} \quad (24)$$

with solution:

$$\delta(\zeta) = \frac{\sinh(\alpha\zeta)}{\sinh(\alpha\bar{\zeta})} + \frac{\Pi\sqrt{\mu}}{\alpha(1-\zeta_r)} \cdot \left\{ 1 - \frac{\sinh(\alpha\zeta) + \sinh[\alpha(\bar{\zeta} - \zeta)]}{\sinh(\alpha\bar{\zeta})} \right\} \quad (25)$$

The second problem holds for the softening zone. Hence the second branch of the interfacial cohesive law (18) must be inserted into the governing eqn (19), while the second boundary condition coincides with the one holding for the elastic stage:

$$\begin{cases} \frac{d^2\delta}{d\zeta^2} - \alpha^2 \frac{\mu - \delta}{\mu - 1} = -\frac{\alpha\sqrt{\mu}}{1-\zeta_r} \Pi, & \bar{\zeta} < \zeta \leq \zeta_r \\ \delta(\bar{\zeta}) = 1, \quad \delta'(\zeta_r) = \Pi\alpha\sqrt{\mu} \end{cases} \quad (26)$$

with solution:

$$\delta(\zeta) = \mu - \frac{\mu - 1}{\cos \alpha_2(\zeta_r - \bar{\zeta})} \left\{ \cos \alpha_2(\zeta_r - \zeta) + \frac{\Pi\sqrt{\mu}}{\alpha(1-\zeta_r)} \left[ \alpha_2(1-\zeta_r) \sin \alpha_2(\zeta - \bar{\zeta}) + \cos \alpha_2(\zeta_r - \zeta) - \cos \alpha_2(\zeta_r - \bar{\zeta}) \right] \right\} \quad (27)$$

where, for the sake of simplicity, we introduced the quantity  $\alpha_2 = \alpha / \sqrt{\mu - 1}$ .

At the elastic-softening stage the load corresponding to each value of  $\bar{\zeta}$  is determined by the condition of stress continuity in the FRP at the boundary between the elastic and softening regions. According to eqn (15), this condition corresponds to

enforcing the continuity of the first derivative of the displacement field at  $\zeta = \bar{\zeta}$ , i.e.:

$$\sigma_r(\bar{\zeta}^+) = \sigma_r(\bar{\zeta}^-) \Rightarrow \delta'(\bar{\zeta}^+) = \delta'(\bar{\zeta}^-) \quad (28)$$

which yields:

$$\Pi = \frac{\alpha(1-\zeta_r)}{\sqrt{\mu}} \cdot \left\{ 1 + \frac{\alpha(1-\zeta_r)\sec[\alpha_2(\zeta_r - \bar{\zeta})] - \operatorname{csech}(\alpha\bar{\zeta})}{\sqrt{\mu-1} \tan[\alpha_2(\zeta_r - \bar{\zeta})] + \operatorname{ctanh}(\alpha\bar{\zeta})} \right\}^{-1} \quad (29)$$

The maximum load  $\Pi_{\max}$  is attained during the elastic-softening stage. In order to compute the position  $\zeta_{\max}$  of the peak stress at which the load reaches its maximum value, it is sufficient to compute the first derivative of eqn (29) and set it to zero. Analytical manipulations lead to the following simple implicit equation in  $\zeta_{\max}$ :

$$\tanh(\alpha\zeta_{\max}) \tan[\alpha_2(\zeta_r - \zeta_{\max})] = \sqrt{\mu-1} \quad (30)$$

which has to be solved numerically for roots in the range  $\zeta_{23} < \zeta_{\max} < \zeta_r$ . The maximum load is finally computed by setting  $\bar{\zeta} = \zeta_{\max}$  in eqn (29). Note that, in case of multiple solutions, the largest root (i.e. the closest to  $\zeta_r$ ) has to be considered when solving eqn (30). On the other hand, the possible absence of a solution means that the load increases monotonically during the debonding process and no snap-through instability arises (see Section 6).

In many practical cases, the quantity  $(\alpha \times \zeta_{\max})$  is much larger than unity, so that the hyperbolic tangent in eqn (30) can be set equal to 1 in engineering calculations. Hence, from eqn (30) the value of  $\zeta_{\max}$  can be achieved explicitly. Its substitution in eqn (29) provides the following approximate expression of the debonding load:

$$\Pi_{\max} = \frac{P_{\max}}{P_{\text{LEFM}}} \cong \left[ 1 + \frac{\sqrt{\mu}}{\alpha(1-\zeta_r)} \right]^{-1} \quad (31)$$

Since the right hand side is always smaller than unity, we conclude that the critical load estimate provided by LEFM is always larger than the one given by the cohesive crack model. The unconditional application of LEFM is therefore potentially dangerous. Note

that the difference between the two predictions vanishes for an infinitely stiff interface ( $\alpha \rightarrow \infty$ ), while it is more pronounced for relatively ductile interfacial behavior (high  $\mu$  value).

Eqn (31) was already derived in [16]. With respect to the exact value given by eqns (29-30), eqn (31) yields very accurate results provided that the softening branch after the peak is relatively sharp. For a mild softening branch, peak load predictions by eqn (31) are less accurate, finally becoming physically meaningless in case of a monotonically increasing load, i.e. when the peak disappears. However, this condition is met only for rather ductile interfaces, as will be shown in Section 6.

### 5.3 Elastic-softening-debonding stage

The third and last stage begins when the relative displacement at the FRP edge reaches the maximum value  $s_r$ , after which the reinforcement is completely detached from the concrete support. In dimensionless form, the debonding starts when  $\delta(\zeta_r) = \mu$ . According to eqns (27) and (29), this condition is met when the position  $\bar{\zeta}$  of the peak load is the root of the following equation:

$$\begin{aligned} \alpha(1-\zeta_r)\sin[\alpha_2(\zeta_r - \bar{\zeta})] - \cos[\alpha_2(\zeta_r - \bar{\zeta})] &= \\ = \frac{\alpha(1-\zeta_r)\sec[\alpha_2(\zeta_r - \bar{\zeta})] - \operatorname{csech}(\alpha\bar{\zeta})}{\sqrt{\mu-1} \tan[\alpha_2(\zeta_r - \bar{\zeta})] + \operatorname{ctanh}(\alpha\bar{\zeta})} \end{aligned} \quad (32)$$

where, in case of multiple roots, the largest value (denoted as  $\zeta_{23}$ ) has to be taken.

During the third and last stage, the initial coordinate of the detached portion of the plate moves gradually from the FRP edge towards the mid-span. Correspondingly, the position  $\bar{\zeta}$  of the stress peak travels from  $\zeta_{23}$  to 0. However it is not necessary to solve any additional differential problem, since the solution is the same as in a strengthened beam of reduced reinforced length at the end of the second stage.

From a computational point of view, this stage can be followed by letting  $\zeta_r$  (which is now the controlling parameter) vary from the initial value to 0. The corresponding position

$\bar{\zeta}$  of the peak stress is hence obtained by solving eqn (32) for any  $\zeta_r$  value and the related load is given once more by eqn (29). Care needs to be taken in normalization: since the dimensionless load provided by eqn (29) refers to the actual reinforcement length  $z_{r,act}$ , the load normalized with respect to eqn (5) (related to the initial reinforcement length  $z_r$ ) is achieved multiplying the result by the ratio  $(l-z_{r,act})/(l-z_r)$ .

## 6 LOAD VS. DISPLACEMENT CURVE AND POST-PEAK INSTABILITIES

Aim of the present section is to obtain the load vs. mid-span displacement curve for a strengthened beam under TPB during the different stages of the interfacial behavior. In order to evaluate the mid-span deflection we start from the beam curvature  $\chi_b$ , which, according to eqns (14) and (15) is given by:

$$\chi_b(z) = \frac{-6\rho}{(1+4\rho)h_b} \left[ \frac{P(l-z)(1+\rho)}{h_b t_r h_r E_r} + \frac{ds}{dz} \right] \quad (33)$$

By integration we obtain the rotation  $\varphi_b$  of the generic cross section as:

$$\varphi_b(z) = \frac{-6\rho}{(1+4\rho)h_b} \left[ \frac{Pz(l-z/2)(1+\rho)}{h_b t_r h_r E_r} + s(z) \right] \quad (34)$$

Neglecting shear deformability in the concrete beam,  $\varphi_b = -v'$ . The transverse displacement is thus given by:

$$v(z) = -\int_z^l \varphi(z) dz \quad (35)$$

The desired value of the mid-span deflection is obtained for  $z = 0$ . For the sake of simplicity we denote simply with  $v$  this value, equal to:

$$v(z=0) = v = \frac{P(2l)^3}{48E_b I} + \frac{6\rho}{1+4\rho} \frac{l}{h_b} s_p \int_0^1 \delta(\zeta) d\zeta \quad (36)$$

where the first term on the right-hand side represents the mid-span deflection that would be obtained from the EB model if the beam were strengthened over its entire length. Some analytical manipulations allow us to rewrite eqn (36) as:

$$v = v_{EB} + \frac{6\rho}{1+4\rho} \frac{l}{h_b} s_p \left[ \int_0^{\zeta_r} \delta(\zeta) d\zeta + (1-\zeta_r)\delta(\zeta_r) \right] \quad (37)$$

where now the first term is exactly the mid-span displacement given by the EB model (see eqn (6)). The second term is the increment in deformability due to the compliance of the interface. Obviously, for an infinitely stiff interface, the relative displacement vanishes ( $\delta \equiv 0$ ) and the mid-span deflection coincides with the one predicted by the EB model.

The mid-span displacement is finally computed, for the various behavioral stages of the interface, upon substitution of the relative displacement field  $\delta(\zeta)$  (eqns (22), (25) and (27)) into eqn (37). It is worth noting that, during the second and third stages, the integral has to be split into two parts, one for the elastic and one for the softening regions:

$$\int_0^{\zeta_r} \delta(\zeta) d\zeta = \int_0^{\bar{\zeta}} \delta(\zeta) d\zeta + \int_{\bar{\zeta}}^{\zeta_r} \delta(\zeta) d\zeta \quad (38)$$

The integrals in eqn (38) can be easily computed analytically. Since their explicit expressions are rather long, they are omitted herein but will be provided integrally in a forthcoming paper.

As done in Section 2, the load and the mid-span deflection can be normalized with respect to their values at the onset of debonding evaluated according to LEFM. While the LEFM curve depends only on the relative bond length  $\zeta_r$  and the mechanical reinforcement fraction  $\rho$  (which govern the difference in slope between the initial strengthened configuration and the final unstrengthened geometry), the load vs. displacements curves obtained by the cohesive crack modeling depend also on the dimensionless parameters  $\alpha$  (eqn (20)) and  $\mu$  (eqn (18)). While the former one is a function of the geometric and elastic properties of the materials, the latter one ( $\mu \geq 1$ ) describes the structural behavior of the interface ( $\mu = 1$  describing an elastic-perfectly brittle interface and  $\mu \rightarrow \infty$  an elastic-perfectly plastic interface). In this preliminary parametric

analysis, we investigate the effect of this second parameter, fixing the other ones to the following values:  $\rho = 0.4$ ;  $\zeta_r = 0.7$ ;  $\alpha = 10$ . The relatively high and somehow unrealistic  $\rho$  value has been chosen to emphasize the difference between the initial and final elastic stiffness, so that the plots are easier to understand.

For the parameter  $\mu$  we chose the following values: 6, 12, 24. The corresponding interfacial cohesive laws are plotted in Fig. 5, denoting a more ductile behavior as  $\mu$  increases.

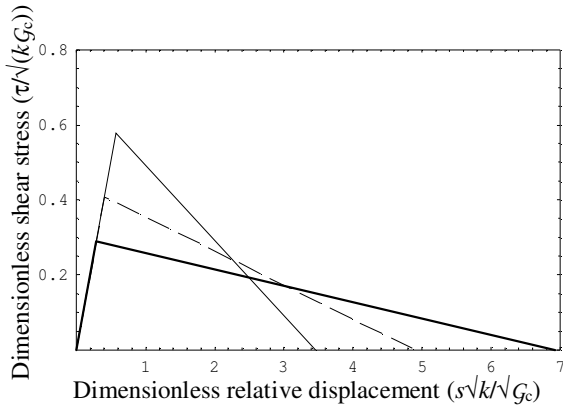


**Figure 5:** Interfacial cohesive law with fixed elastic stiffness and fracture energy:  $\mu = 6$  (thin line),  $\mu = 12$  (dashed line),  $\mu = 24$  (thick line).

The three load vs. mid-span deflection curves corresponding to the three  $\mu$  values are plotted in Fig. 6. In each figure, the LEFM prediction has also been plotted for the sake of comparison. It is evident that the cohesive crack model predicts a less brittle response with respect to LEFM, thus evidencing a less catastrophic structural behavior. However it is worth noting that the peak load (a local maximum in this case, the beam material being considered infinitely strong) is always lower than the one predicted by LEFM, whose application must hence be considered as unconservative. Note also that the present cohesive model collapses onto the LEFM model for  $\mu \rightarrow 1$  (elastic-perfectly brittle interface) and  $\alpha \rightarrow \infty$  (infinite stiffness interface).

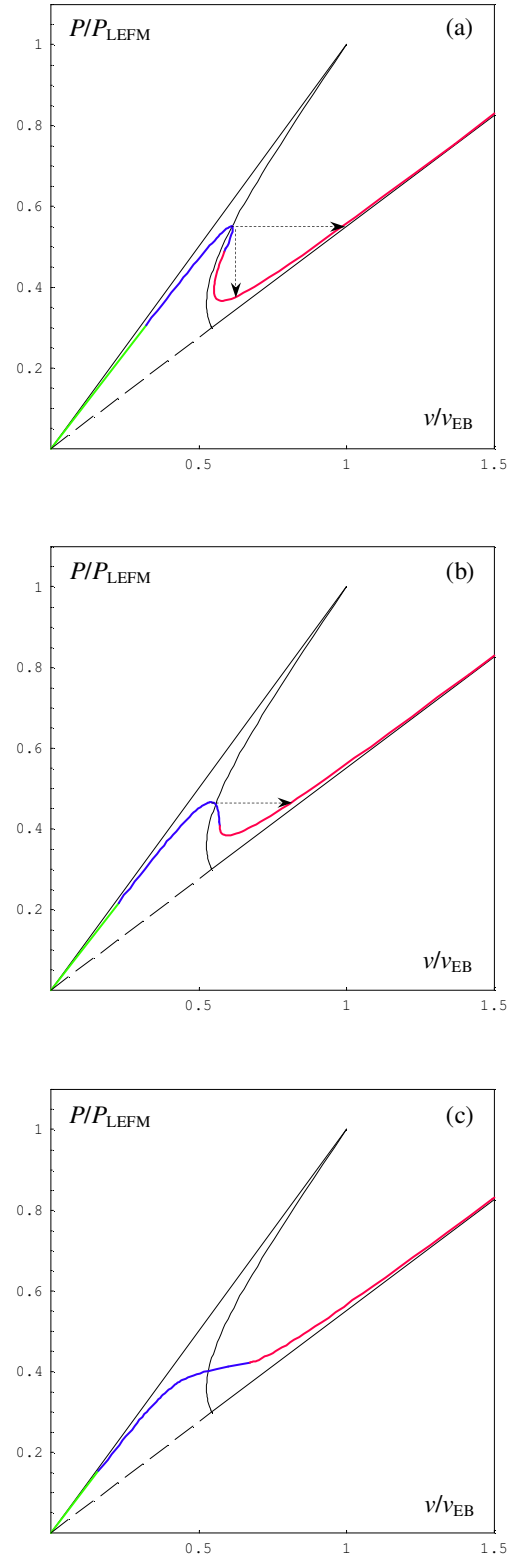


**Figure 6:** Load vs. displacement curves for  $\mu = 6$  (a),  $\mu = 12$  (b) and  $\mu = 24$  (c). The arrows denote possible instabilities according to the test control.

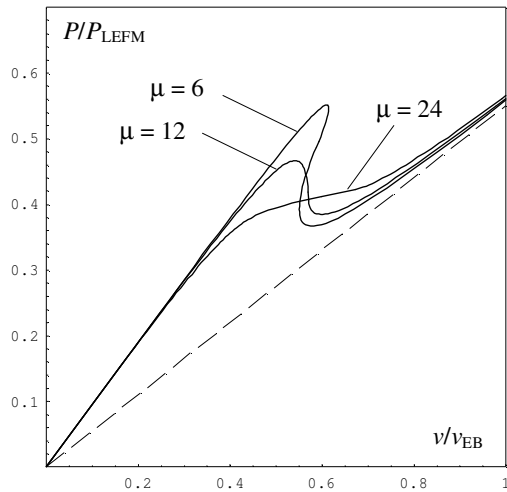


**Figure 7:** Dimensionless load vs. displacement curves for  $\mu = 6, 12, 24$ .

In Fig. 6 the lines referring to the elastic stage are marked in green; the blue portions of the curves correspond to the elastic-softening stage (where the peak is achieved); the red branches are related to the elastic-softening-debonding stage. Since the fracture energy is fixed (see Fig. 5), the area between the load-displacement curves and the straight line corresponding to the unreinforced structure is the same for all curves, being proportional to the energy spent to obtain the complete detachment of the FRP plate from the concrete substrate.

As far as the post-peak instabilities are concerned, we note that for sufficiently brittle interface (e.g. for  $\mu = 6$ , see Fig. 6a), both the snap-back and the snap-through instabilities may occur, since the softening branch contains a region with positive slope. The slope of the softening branch becomes entirely negative for  $\mu \geq 11$ , therefore only the snap-through instability appears if the test is load-controlled (see Fig. 6b, where  $\mu = 12$ ). For higher  $\mu$  values ( $\mu \geq 21$ ), the load-displacement curve is monotonically increasing and no instabilities are to be expected (as in Fig. 6c, where  $\mu = 24$ ). For the sake of comparison, in Fig. 7 the three load-displacement curves have been plotted on the same graph.

## 7 CONCLUSIONS

In this paper we presented an analytical approach for prediction of the edge debonding of a thin FRP plate from the soffit of a concrete beam. The approach is based on cohesive crack modeling of the interface between FRP and concrete. The analysis is an extension of previous results of the same authors [7, 16], but it can also be seen as an extension of previous studies dealing with the (simpler) pull-push geometry (e.g. [8]) to debonding failure under TPB loading.

After deriving the analytical expressions of the relative displacement between the reinforcement and the beam intrados, the attention was focused on the global structural behavior of a strengthened beam under TPB, as well as on the instability mechanisms that may occur. We further showed that simple LEFM predictions of the failure load are unconservative, thus justifying the need for the proposed more refined approach.

## ACKNOWLEDGEMENTS

The Authors acknowledge the financial support of the Italian Ministry of Education, University and Research to the project ‘‘Advanced applications of fracture mechanics for the study of integrity and durability of materials and structures’’ within the PRIN program for the year 2008.

## REFERENCES

- [1] Carpinteri, A., Cornetti, P., Lacidogna, G. and Paggi, M., 2009. Towards a unified approach for the analysis of failure modes in FRP-retrofitted concrete beams. *Adv. Struct. Eng.* **12**:715-29.
- [2] De Lorenzis, L., 2012. Some recent results and open issues on interface modeling in civil engineering structures. *Mater. Struct.* **45**:477-503
- [3] Taljsten, B., 1997. Strengthening of beams by plate bonding. *J. Mater. Civ. Eng.-ASCE* **9**:206-12.
- [4] Smith, S. and Teng, J., 2001. Interfacial

- stresses in plated beams. *Eng. Struct.* **23**: 857-71.
- [5] Rabinovitch, O., 2004. Fracture-mechanics failure criteria for RC beams strengthened with FRP strips - a simplified approach. *Compos. Struct.* **64**:479-92.
- [6] Colombi, P., 2006. Reinforcement delamination of metallic beams strengthened by FRP strips: Fracture mechanics based approach. *Eng. Fract. Mech.* **73**:1980-95.
- [7] Carpinteri, A., Cornetti, P., and Pugno, N., 2009. Edge debonding in FRP strengthened beams: Stress versus energy failure criteria. *Eng. Struct.* **31**:2436-47.
- [8] Yuan, H., Teng, J.G., Seracino, R., Wu, Z.S. and Yao, J., 2004. Full-range behavior of FRP-to-concrete bonded joints. *Eng. Struct.* **26**: 553-65.
- [9] Leung, C.K.Y. and Tung, W.K., 2006. Three-parameter model for debonding of FRP plate from concrete substrate. *J. Eng. Mech.-ASCE* **132**:509-18.
- [10] Cottone, A. and Giambanco, G., 2009. Minimum bond length and size effects in FRP-substrate bonded joints. *Eng. Fract. Mech.* **76**:1957-76.
- [11] Carpinteri, A., and Cornetti, P., 2011. Modelling the FRP-concrete delamination by means of an exponential softening law. *Eng. Struct.* **33**:1988-2001.
- [12] Caggiano, A., Martinelli, E. and Faella, C., 2012. A fully-analytical approach for modelling the response of FRP plates bonded to a brittle substrate. *Int. J. Solids Struct.* **49**:2291-300
- [13] Ferracuti, B., Savoia, M. and Mazzotti, C., 2006. A numerical model for FRP-concrete delamination. *Compos. Pt. B-Eng.* **37**:356-64.
- [14] Dehghani, E., Daneshjoo, F., Aghakouchak, A.A. and Khaji, N., 2012. A new bond-slip model for adhesive in CFRP-steel composite systems. *Eng. Struct.* **34**:447-54.
- [15] Rabinovitch, O., 2008. Debonding analysis of fiber-reinforced-polymer strengthened beams: cohesive zone modeling versus a linear elastic fracture mechanics approach. *Eng. Fract. Mech.* **75**:2842-59.
- [16] De Lorenzis, L., and Zavarise, G., 2009. Cohesive zone modeling of interfacial stresses in plated beams. *Int. J. Solids Struct.* **46**:4181-91.
- [17] Bennati, S., Dardano, N. and Valvo, P. S., 2011. Un modello meccanico per travi inflesse rinforzate con FRP. In *Proceedings of the XXI National Conference of the Italian Group of Fracture (IGF XXI)*, June 13-15, 2011, Cassino, Italy, pp. 360-74.
- [18] Carpinteri, A. and Paggi, M., 2010. Analysis of snap-back instability due to end-plate debonding in strengthened beams. *J. Eng. Mech.-ASCE* **136**:199-208.